THE JOURNAL OF BIOLOGICAL CHEMISTRY VOL. 286, NO. 31, pp. 27436–27446, August 5, 2011

External Cu^{2+} Inhibits Human Epithelial Na^+ Channels by Binding at a Subunit Interface of Extracellular Domains*

Received for publication, February 16, 2011, and in revised form, June 3, 2011 Published, JBC Papers in Press, June 9, 2011, DOI 10.1074/jbc.M111.232058

Jingxin Chen, Mike M. Myerburg, Christopher J. Passero, Katie L. Winarski, and Shaohu Sheng[1]

From the Department of Medicine, School of Medicine, University of Pittsburgh, Pittsburgh, Pennsylvania 15261

Epithelial Na^+ channels (ENaCs) play an essential role in the regulation of body fluid homeostasis. Certain transition metals activate or inhibit the activity of ENaCs. In this study, we examined the effect of extracellular Cu^{2+} on human ENaC expressed in *Xenopus* oocytes and investigated the structural basis for its effects. External Cu^{2+} inhibited human $\alpha\beta\gamma$ ENaC with an estimated IC_{50} of 0.3 μM. The slow time course and a lack of change in the current-voltage relationship were consistent with an allosteric (non pore-plugging) inhibition of human ENaC by Cu^{2+}. Experiments with mixed human and mouse ENaC subunits suggested that both the α and β subunits were primarily responsible for the inhibitory effect of Cu^{2+} on human ENaC. Lowering bath solution pH diminished the inhibition by Cu^{2+}. Mutations of two α, two β, and two γ His residues within extracellular domains significantly reduced the inhibition of human ENaC by Cu^{2+}. We identified a pair of residues as potential Cu^{2+}-binding sites at the subunit interface between thumb subdomain of αhENaC and palm subdomain of βhENaC, suggesting a counterclockwise arrangement of α, β, and γ ENaC subunits in a trimeric channel complex when viewed from above. We conclude that extracellular Cu^{2+} is a potent inhibitor of human ENaC and binds to multiple sites within the extracellular domains including a subunit interface.

The epithelial Na^+ channel (ENaC)[2] mediates Na^+ transport across apical membranes of high resistance epithelia in kidney, colon, and lung. ENaC has important roles in the maintenance of extracellular fluid volume and the regulation of airway surface liquid volume (1). Alterations in ENaC activity have been associated with several human diseases. For example, enhanced ENaC activity is responsible for the hypertension seen in Liddle's syndrome, contributes to the mucociliary dysfunction seen in cystic fibrosis, and is believed to contribute to hypervolemia associated with nephrotic syndrome (2, 3).

A variety of intracellular and extracellular factors regulate ENaC activity by distinct mechanisms (4). External amiloride analogs, cations, anions, nucleotides, serine proteases, and laminar shear stress inhibit or stimulate endogenous or exogenous ENaCs (5–12). All of these extracellular regulators appear to directly alter the activity of ENaCs in plasma membranes rather than affect channel subunit trafficking (1). Their primary targets likely reside within the characteristically large extracellular domains (ECDs) of ENaC subunits. This notion is in line with the well defined subdomains within the ECDs of the chicken acid-sensing ion channel 1 (cASIC1), a member of the ENaC/degenerin family, revealed in a crystal structure and the identification of proton binding sites within the ECDS (13).

We have previously examined the effects of the transition metals, Ni^{2+} and Zn^{2+}, on ENaC activity. External Ni^{2+} inhibits and Zn^{2+} activates mouse ENaCs in *Xenopus* oocytes by directly interacting with the channels and altering channel gating (6, 7). Some of these metal effects are thought to be related to Na^+ self-inhibition, a down-regulation of open probability (P_o) by extracellular Na^+ (7, 14). Yu *et al.* (14) have also examined the effects of several transition metals on the single channel activity of native *Xenopus* ENaCs in A6 cells. These metals differentially affect *Xenopus* ENaC Po and channel number in membrane patches without changing the single channel conductance. However, the exact binding sites and detailed mechanisms for the metal effects on ENaCs remain largely unknown.

Copper is the third most abundant trace metal in humans and has a variety of important biological functions. Excessive Cu^{2+} is highly toxic to cells, and its content in cells is carefully maintained at low levels. Indeed, Cu^{2+} is implicated in several human diseases such as Wilson disease, Menkes disease, neurodegenerative disorders, and cancers (15, 16). The therapeutic potential of copper chelators and copper complexes is being intensively investigated (16). In addition, particulate matters contain high amounts of transitional metals including copper. Soluble metals in airborne particles contribute to pulmonary and cardiovascular toxicity (17, 18). Recent studies suggest that copper nanoparticles are highly toxic (19). The underlying mechanisms for the harmful effects of Cu^{2+} are not fully understood. Many studies have suggested that certain metals exert their toxic effects in part by altering functions of ion channels or transporters (20, 21). Clearly, a better understanding of the interactions between copper and biological molecules is crucial to an elucidation of its physiological, pathological, and toxicological roles in human health.

In this report, we examined the effects of external Cu^{2+} on amiloride-sensitive Na^+ currents in oocytes expressing $\alpha\beta\gamma$ human ENaC (hENaC) and probed the structural basis by site-directed mutagenesis. We found that external Cu^{2+} is a potent inhibitor of hENaC. The inhibitory effect of Cu^{2+} on hENaC

* This work was supported, in whole or in part, by National Institutes of Health Grants R01 ES014701, K08 HL087932, P30 DK072506, and P30 DK079307. This work was also supported by a research grant from Dialysis Clinic, Inc. and the Cystic Fibrosis Foundation RDP to the University of Pittsburgh.

[1] To whom correspondence should be addressed: Renal-Electrolyte Division, University of Pittsburgh, S929 Scaife Hall, 3550 Terrace St., Pittsburgh, PA 15261. Tel.: 412-648-9295; Fax: 412-383-8956; E-mail: shaohu@pitt.edu.

[2] The abbreviations used are: ENaC, epithelial Na^+ channel; hENaC, human ENaC; mENaC, mouse ENaC; ASIC, acid sensing ion channel; ECD, extracellular domain; MES, 2-(*N*-morpholino) ethanesulfonic acid; MOPS, 3-(*N*-morpholino) propanesulfonic acid; TTM, tetrathiomolybdate.

depends on the α and β subunits. The most important site for Cu^{2+} inhibition was identified at the α/β subunit interface.

EXPERIMENTAL PROCEDURES

cDNA Constructs and Site-directed Mutagenesis—Wild-type α, β, and γ hENaC cDNAs (22, 23) were in pSPORT, pBluescript KS+, and pCDNA3 vectors, respectively. Point mutations were introduced into hENaC cDNAs using the QuikChange II XL site-directed mutagenesis kit (Stratagene). The presence of intended mutations and the absence of unwanted mutations were verified by direct DNA sequencing. Mouse α, β, and γ ENaC (mENaC) cDNAs were in pBluescript SK− vector. Wild-type and mutant hENaC cRNAs were made using SP6 (αhENaC) or T7 (β and γ hENaC) RNA polymerase (Ambion, Inc.). All of the mENaC cRNAs were made using T3 RNA polymerase (Ambion, Inc.). The synthesized cRNAs were purified with an RNA purification kit (Qiagen) and quantified by spectrophotometry.

ENaC Expression and Two-electrode Voltage Clamp—ENaC expression in *Xenopus* oocytes and current measurements by two-electrode voltage clamp were performed as previously reported (6). Stage V and VI oocytes with the follicle cell layer removed were injected with 50 nL/cell of mixed cRNAs composed of 2 ng of each hENaC subunit or 1 ng of each mENaC subunit. Injected oocytes were incubated at 18 °C in modified Barth's solution (88 mM NaCl, 1 mM KCl, 2.4 mM $NaHCO_3$, 15 mM HEPES, 0.3 mM $Ca(NO_3)_2$, 0.41 mM $CaCl_2$, 0.82 mM $MgSO_4$, 10 μg/ml of sodium penicillin and streptomycin sulfate, 100 μg/ml gentamycin sulfate, pH 7.4). All of the experiments were performed at room temperature (20–24 °C) 20–30 h following injection. The oocytes were placed in a recording chamber from Warner Instruments (Hamden, CT) and perfused with bath solutions at a constant flow rate of 12–15 ml/min. Voltage clamp was performed using Axoclamp 900A amplifier and DigiData 1440A interface controlled by pClamp 10 (Molecular Devices Corporation, Sunnyvale, CA). The oocytes were either continuously clamped to −100 mV to monitor current change over a period of time or stepwise clamped to a series of voltages (−140 to 60 mV) to determine the current-voltage relationship.

Examination of the Effects of Cu^{2+} on ENaCs in Oocytes— The oocytes were perfused with normal bath solution (NaCl-110, containing 110 mM NaCl, 2 mM KCl, 2 mM $CaCl_2$, pH 7.4) while clamped to −100 mV. Bath solution was buffered with either 10 mM HEPES or 5 mM MES and 5 mM MOPS. Although HEPES reportedly forms complex with Cu^{2+} (24), we observed similar responses to Cu^{2+} using bath solution buffered with either HEPES or MES and MOPS that do not complex Cu^{2+}. Inward currents were continuously recorded, whereas bath solutions supplemented with or without Cu^{2+} were exchanged. Following Cu^{2+} washout, bath solution was switched to NaCl-110 with 10 μM amiloride to determine the amiloride-insensitive current. The effects of Cu^{2+} on ENaCs were analyzed by comparison of the amiloride-sensitive currents prior to and after Cu^{2+} application. A Cu^{2+} stock solution of 1 M was prepared by dissolving $CuSO_4{\cdot}5H_2O$ (purity of 99.999%; Sigma-Aldrich) in deionized water and was diluted to its final concentration in NaCl-110. The highest concentration of Cu^{2+} solution that could be made in this bath solution and remain relatively stable was 100 μM, and precipitates appeared at higher concentration. Bath solutions containing Cu^{2+} were prepared fresh prior to experiments to minimize the reduction of Cu^{2+} concentration because of the slow formation of insoluble $Cu(OH)_2$ at neutral pH. Nominal concentrations of Cu^{2+} were used. Oocytes with unstable currents were not used in these experiments.

Examination of Na^+ Self-inhibition—The Na^+ self-inhibition responses were examined as previously reported (25, 26). Briefly, Na^+ self-inhibition was examined by rapidly replacing a low [Na^+] bath solution (NaCl-1; containing 1 mM NaCl, 109 mM *N*-methyl-D-glutamine (NMDG), 2 mM KCl, 2 mM $CaCl_2$, 10 mM HEPES, pH 7.4) with a high [Na^+] bath solution (NaCl-110), whereas the oocytes were continuously clamped to −100 mV. Bath solution exchange was done with a Teflon valve perfusion system controlled by computer (AutoMate Scientific Inc, Berkeley, CA). Upon completion of the experiment, 10 μM amiloride was added to the bath solution so as to determine the amiloride-insensitive portion of the whole cell current. To avoid complications from the observable variability in the Na^+ self-inhibition response of WT ENaCs among different batches of oocytes (27), the response of WT channels was always tested in an alternating manner with mutants in the same batch of oocytes. Steady state current (I_{ss}) was measured at 40 s after I_{peak}. The amiloride-insensitive currents were subtracted from I_{ss} and I_{peak} currents to determine the amiloride-sensitive current ratio of I_{ss}/I_{peak}, the index for the magnitude of Na^+ self-inhibition.

Examination of the Effect of Cu^{2+} on hENaCs in Human Airway Epithelial Monolayer—Primary human airway epithelial cells were cultured from excess pathological tissue following lung transplantation and organ donation under a protocol approved by the University of Pittsburgh Investigational Review Board. Human airway epithelial cells were cultured on human placental collagen-coated Costar Transwell filters (0.33 cm^2) as described previously (28) and used for experimentation following 4–6 weeks of culture at an air-liquid interface. Short circuit currents (I_{sc}) were measured as previously described (28). In brief, cells cultured on filter supports were mounted in modified Ussing chambers, and the cultures were continuously short circuited with an automatic voltage clamp (Physiologic Instruments). The bathing Ringer's solution was composed of 120 mM NaCl, 10 mM HEPES, 3.3 mM KH_2PO_4, 0.8 mM K_2HPO_4, 0.6 mM $MgCl_2$, 0.6 mM $CaCl_2$, and 10 mM glucose (pH, 7.4). Chambers were constantly gassed with a mixture of 95% O_2 and 5% CO_2 at 37 °C, which maintained a pH of 7.35. Simultaneous transepithelial resistance was recorded by applying a 10-mV pulse/s via an automated pulse generator. Acquire and Analyze 2.3 (Physiological Instruments) was used to control the voltage clamp and analyze the I_{sc} data. I_{sc} recordings included a 30-min equilibration period, followed by the addition of Cu^{2+} from a 1 M Cu^{2+} stock solution in water, followed by the addition of 20 μM amiloride.

Statistical Analysis—The data are presented as the means ± S.E. Significance comparisons between groups were performed using Student's *t* test. Curve fittings were performed with Origin Pro 8.0 (OriginLab Corporation, Northampton, MA).

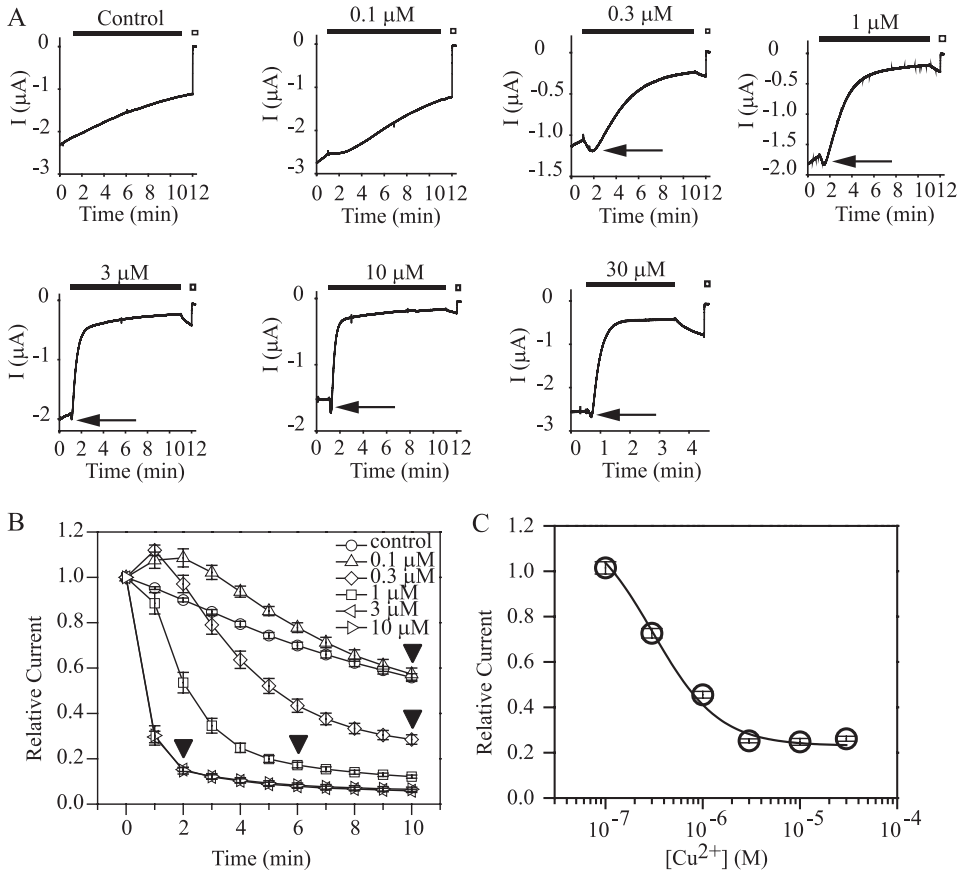

FIGURE 1. **External Cu^{2+} inhibits human ENaC.** *A*, representative recordings of whole cell currents from oocytes expressing $\alpha\beta\gamma$ hENaCs before, during, and after Cu^{2+} applications. Each trace represents at least five independent observations. The oocytes were clamped at −100 mV. Cu^{2+} was added to the bath solution (NaCl-110 with 110 mM Na^+, buffered with 5 mM MES and 5 mM MOPS) at 0.1, 0.3, 1, 3, 10, and 30 μM. Control oocytes were clamped in the same way except no Cu^{2+} application. Inward currents were shown in negative values by convention. The durations of Cu^{2+} and amiloride (10 μM) applications are indicated by *black* and *open bars*, respectively. *Black arrows* point to the transient increases in currents after initiation of Cu^{2+} applications. *B*, time courses of the current changes in the absence (control) or presence of Cu^{2+}. The relative currents were the ratios of the amiloride-sensitive currents measured every minute after the beginning of the Cu^{2+} applications and the amiloride-sensitive currents prior to Cu^{2+} additions (at time 0). The data were from 17 oocytes for control and 9 or 10 oocytes for Cu^{2+} applications. The *black arrowheads* indicate the times when datum points were chosen for dose-response analysis (2 min for 3 and 10 μM Cu^{2+}, 5 min for 1 μM Cu^{2+}, and 10 min for 0.1 and 0.3 μM Cu^{2+}). *C*, dose response of Cu^{2+} on $\alpha\beta\gamma$ hENaCs. The relative currents from *B* were adjusted to deduct rundown contribution from the observed current decreases at the corresponding time with the formula: I_R (corrected) = $I_R + (1 - I_{R\ control})$. I_R and $I_{R\ control}$ were the relative currents with and without Cu^{2+}, respectively. The line was from a best fit with the Hill equation. The parameters were: IC_{50}, 0.31 μM; *n*, 1.28, *B*, 0.23; and R^2, 0.99.

RESULTS

External Cu^{2+} Inhibits Human $\alpha\beta\gamma$ ENaC—We examined the effect of extracellular Cu^{2+} on whole cell currents in *Xenopus* oocytes expressing $\alpha\beta\gamma$ hENaC. Oocytes were continuously clamped at −100 mV to monitor inward current changes before, during (10 min), and after Cu^{2+} application in bath solution (NaCl-110 buffered with 5 mM MES and 5 mM MOPS). Because ENaC activity in oocytes typically experiences a rundown (*i.e.* a spontaneous decline of current over time) (29, 30), control experiments were performed the same way except with no Cu^{2+} addition. The rundown was nearly linear but best fit with an exponential equation. The estimated time constant was 736.6 ± 67.2 s (n = 13). In response to external application of 0.1 μM Cu^{2+}, the current increased slightly at first and then declined in a similar way to the control recording (Fig. 1*A*), indicating a lack of inhibitory effect. At higher concentrations, Cu^{2+} reduced the currents in a dose-dependent manner. The time course of the current changes in the absence and presence of Cu^{2+} are shown in Fig. 1*B*, and the estimated time constants are listed in Table 1.

TABLE 1

Time constants for current decreases in the absence (control) and presence of various concentrations of Cu^{2+} in oocytes expressing $\alpha\beta\gamma$ hENaC

Time constants were obtained from best fit of the current changes within 10 min using built-in exponential function in Clampfit 10. The data were from Fig. 1. The time constant for 0.1 μM Cu^{2+} could not be obtained.

[Cu^{2+}]	Tau	Oocytes
	s	
0 μM (control)	736.6 ± 67.2	13
0.1 μM	ND	
0.3 μM	199.9 ± 8.5	7
1 μM	92.1 ± 4.4	8
3 μM	35.7 ± 2.3	10
10 μM	31.8 ± 2.7	9

ND, not determined.

We generated a dose-response curve by plotting the relative currents against Cu^{2+} concentrations (Fig. 1*C*). Measurements were taken at times equivalent to approximately three time constants after the addition of Cu^{2+} (Table 1 and *black arrowheads* in Fig. 1*B*). Time constant for 0.1 μM Cu^{2+} could not be determined; values at 10 min were used. The data for 30 μM Cu^{2+} were taken at 2 min from experiments with Cu^{2+} applied

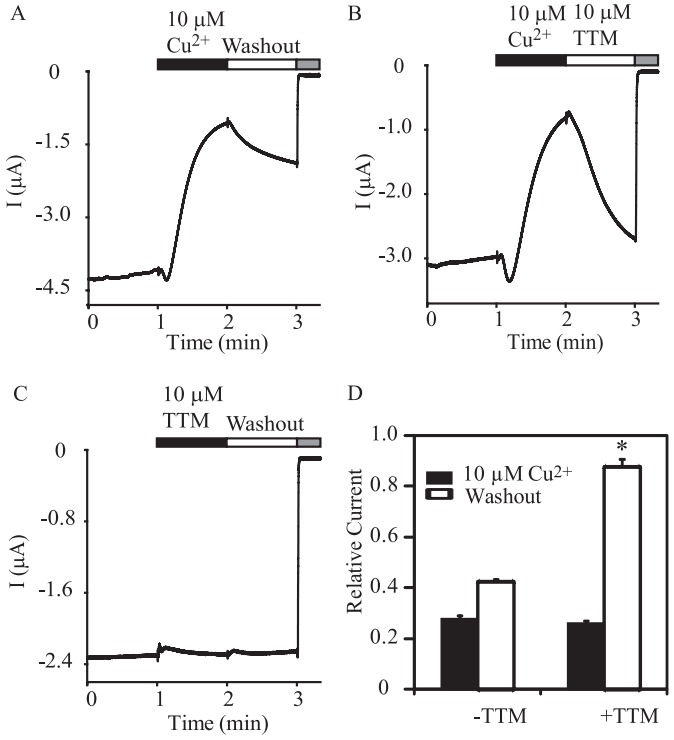

FIGURE 2. **Time course and reversibility of Cu^{2+} inhibition of hENaC.** Seven oocytes expressing $\alpha\beta\gamma$ hENaCs were used for each experiment in *A–C*. *A*, a typical recording showing the current changes following 1 min of application and 1 min of washout of 10 μM Cu^{2+}. *B*, representative recording showing the current changes following 1 min of application of 10 μM Cu^{2+} and 1 min of washout with 10 μM TTM. *C*, representative recording showing effects of 10 μM TTM and its washout on the current. Relative currents (amiloride-sensitive currents after 1 min of application of 10 μM TTM normalized to those prior to TTM treatment) were 0.98 ± 0.02 ($n = 7$, $p > 0.05$ from paired Student's *t* test). *D*, summary data for experiments shown in *A* and *B*. The *asterisk* indicates that the relative current after washout with TTM was significantly higher than that after washout with NaCl-110 ($p < 0.001$). To minimize rundown of ENaC currents typically seen under continuous hyperpolarization, 10 μM Cu^{2+} was applied for only 1 min and washed out for 1 min. The current was approaching a plateau at 1 min of Cu^{2+} application, and the I_{Cu}/I was slightly greater than that with 3 min of application. Bath solution was buffered with 5 mM MES and 5 mM MOPS.

for 3 min (Fig. 1*A*). The relative currents were adjusted to deduct rundown contribution from the observed current decreases at the corresponding time as described in details in the figure legend. Fitting the data with the Hill equation ($I_{Cu}/I = IC_{50}^n/(C^n + IC_{50}^n) + B$, n for Hill coefficient, C for Cu^{2+} concentration, and B for bottom plateau) yielded the following parameters: IC_{50}, 0.31 μM; n, 1.28; and B, 0.23 with the coefficient of determination (R^2) of 0.98.

Prior to the inhibitory effect of Cu^{2+} on hENaC, a small transient increase in current was typically seen (*arrows* in Fig. 1*A*). The transient change in current was not an artifact, although its magnitude varied among different batches of oocytes. It likely resulted from a rapid activation of the channel prior to the inhibitory effect of Cu^{2+}.

The inhibitory effect of Cu^{2+} on hENaCs was not readily reversible. Washout of Cu^{2+} for 1 min only moderately restored the inhibited currents (Figs. 1 and 2*A*). This slow reversal could result from either tight binding of Cu^{2+} to the channel complex or permanent inactivation of channels. To distinguish these two possibilities, we utilized a high affinity Cu^{2+} chelator, tetrathiomolybdate (TTM), to facilitate Cu^{2+} removal from its binding site(s). Inhibition of hENaC by 10 μM Cu^{2+} was nearly completely reversed following the addition of 10 μM TTM (Fig. 2, *B* and *D*). TTM alone did not change the current (Fig. 2*C*). The results suggested that the slow reversibility of Cu^{2+} inhibition reflects tight binding of Cu^{2+} to hENaC.

External Cu^{2+} Inhibits hENaC by Acting on Sites outside of the Pore—Because Cu^{2+} was applied in bath solution in our study, its action site is likely within either the ECD or the transmembrane domain. We carried out experiments to examine these two possibilities. First, we examined the effect of Cu^{2+} on the current-voltage (I-V) relationship of hENaC. As shown in Fig. 3*A*, the I-V curve remained linear following a 3-min application of 10 μM Cu^{2+}. The voltage independence of Cu^{2+} inhibition is inconsistent with a pore blocking effect. A positively charged pore blocker such as amiloride preferentially blocks the inward current causing an outward rectification in the I-V curve (Fig. 3*A*, *curve* for amiloride). Second, we tested whether pore blocker amiloride could protect the channels from inhibition by Cu^{2+}. ENaC currents completely recovered after washout of 10 μM amiloride (Fig. 3, *B* and *D*). However, when oocytes were pretreated with 10 μM amiloride followed by 10 μM Cu^{2+}, currents only partially recovered after washout of both Cu^{2+} and amiloride (Fig. 3, *C* and *D*). Apparently, Cu^{2+} inhibited hENaC current after the pore had been occupied by amiloride. These results suggest that Cu^{2+} acts at a site that is external to the amiloride-binding site within the pore. Based on the above observations, we conclude that external Cu^{2+} inhibits human ENaCs likely by binding to sites outside of the pore.

Human α and β Subunits Are Necessary to Confer the Response of hENaC to Cu^{2+}—We tested whether Cu^{2+} had a similar effect on mouse ENaC and observed that 10 μM Cu^{2+} did not significantly inhibit the current in oocytes expressing $\alpha\beta\gamma$ mENaC (Fig. 4*E*). To determine the hENaC subunits (α, β, and/or γ) that are necessary for Cu^{2+} inhibition, we expressed hybrid channels containing mixed human and mouse subunits in *Xenopus* oocytes. Replacing human α or β subunits with their mouse counterpart significantly reduced the inhibitory effect of 10 μM Cu^{2+}, whereas replacing the γ subunit did not alter the effect of 10 μM Cu^{2+} (Fig. 4). These results suggest that both the α and β subunits are required for the inhibitory effect of Cu^{2+} on hENaC activity.

Mutations of Multiple His Residues within the ECDs Reduce Cu^{2+} Inhibition—We hypothesized that the ECDs of the α and β hENaCs contain residues that are required to confer the inhibitory response to Cu^{2+}. Because Cu^{2+} is often coordinated by side chains of His, Cys, Met, Glu, and Asp (31), we replaced His, Met, Glu, and Asp residues of α or β hENaC to their counterparts seen in mENaC at equivalent sites. All 16 Cys residues within α ECDs and 18 Cys residues within β ECDs are conserved between human and mouse ENaCs and therefore were not included in this analysis. Among nine α mutants, αH468S significantly reduced Cu^{2+} inhibition (Fig. 5*A*). Substitution of αHis^{468} with Cys, Asp, Glu, Lys, or Ala similarly attenuated Cu^{2+} inhibition (Fig. 5, *C* and *D*). Moreover, these mutations also rendered the Cu^{2+} inhibition reversible. Certain mutations at αHis^{468} also decreased the rates of Cu^{2+} inhibition or increased the rates of current recovery following washout (Table 2). Interestingly, αH468C dramatically increased

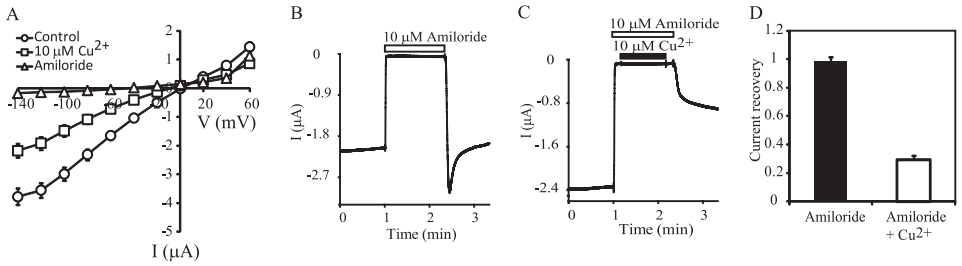

FIGURE 3. **Cu^{2+} binding site is likely not located within hENaC pore.** *A*, I-V curves before and after 10 μM Cu^{2+}. Oocytes expressing $\alpha\beta\gamma$ hENaCs ($n = 5$) were clamped to a series of voltages (−140 to 60 mV) for 500 ms, and the currents were measured at 400 ms. *B*, recording trace showing current changes before, during, and after washout of 10 μM amiloride (80 s). Oocytes were clamped at −100 mV. The current decay from a peak current following amiloride washout reflects Na^+ self-inhibition response (25). *C*, recording from a similar experiment to the one in *B* except that 10 μM Cu^{2+} was co-applied with 10 μM amiloride for 60 s. Cu^{2+} was added 10 s after amiloride and withdrawn 10 s before amiloride to ensure that Cu^{2+} was only applied in the presence of amiloride. Bath solution was buffered with 5 mM MES and 5 mM MOPS. *D*, current recovery after amiloride washout with (*open bar*) or without (*black bar*) Cu^{2+}. The values were the ratios of the amiloride-sensitive currents measured after amiloride washout for 60 s and before amiloride application. The current recovery following co-application of amiloride and Cu^{2+} was significantly lower than that following amiloride application alone ($p < 0.001$, $n = 10$ for amiloride and 7 for amiloride + Cu^{2+}).

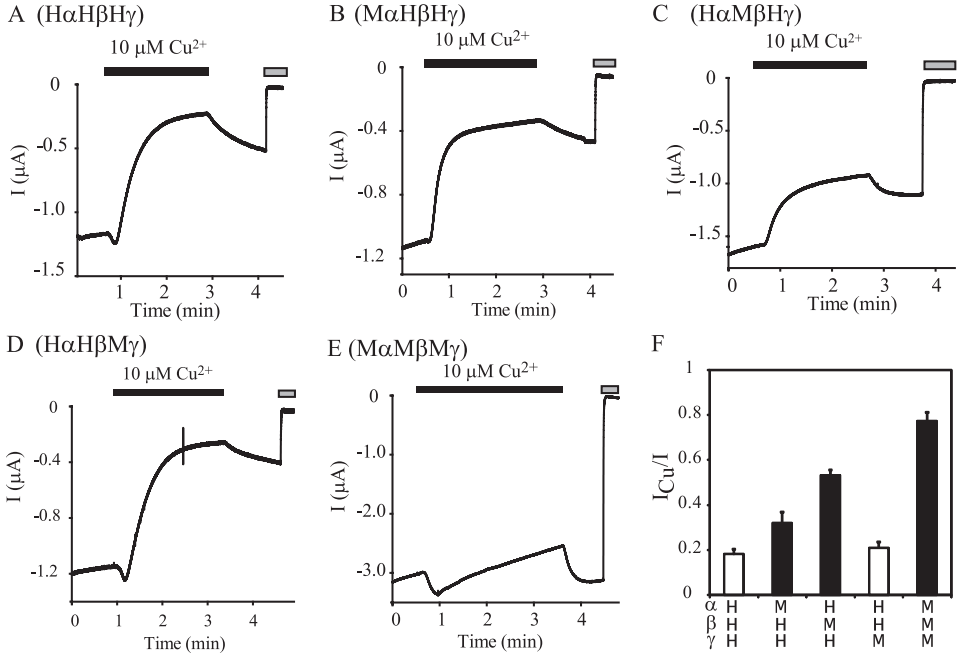

FIGURE 4. **Both α and β subunits contribute to the distinct responses of hENaC and mENaC to external Cu^{2+}.** The effects of 10 μM Cu^{2+} on whole cell currents were examined in oocytes expressing $\alpha\beta\gamma$ hENaC (*A*, HαHβHγ), α mENaC with β and γ hENaC (*B*, MαHβHγ), α and γ hENaC with β mENaC (*C*, HαMβHγ), α and β hENaC and γ mENaC (*D*, HαHβMγ), or $\alpha\beta\gamma$ mENaC (*E*, MαMβMγ). Each recording represents five observations. The *gray bars* show the presence of 10 μM amiloride. *F*, relative current (I_{Cu}/I, $n = 5$). Bath solution was buffered with 10 mM HEPES. The I_{Cu}/I values were the ratios of amiloride-sensitive currents measured after and before 10 μM Cu^{2+} applications. Rundown was not deducted from the observed current decreases in this and all subsequent figures. The *solid bars* indicate that the values are significantly different from that of $\alpha\beta\gamma$hENaC obtained in the same batches of oocytes ($p < 0.05$ for MαHβHγ, $p < 0.001$ for HαMβHγ and MαMβMγ).

both rates, suggesting that the introduced Cys side chain might retain certain capability of this residue interacting with Cu^{2+}. After His, Cys is the second most frequent Cu^{2+} coordinating residue (31). One of the 13 β mutants, βH159D, showed a significantly reduced response to 10 μM Cu^{2+} but did not alter its reversibility or rate (Fig. 5, *B* and *D*). Double mutant αH468S-βH159D showed a minimal inhibitory response to 10 μM Cu^{2+} ($I_{Cu}/I = 0.85 \pm 0.01$, $n = 6$, $p <$ 0.0001 *versus* WT; Fig. 5).

Histidine has an ionizable imidazole ring with an average pK_a of 6.6 ± 1.0 in folded proteins (32). If His residues are indeed involved in Cu^{2+} inhibition of hENaC, lowering the pH of the bath solution containing Cu^{2+} should reduce Cu^{2+} inhibition because of increased protonation of imidazole nitrogens. We therefore examined the effect of 10 μM Cu^{2+} in pH 6.0 bath solution on hENaC currents. Changing the pH of the bath solution from 7.4 to 6.0 moderately increased currents in oocytes expressing $\alpha\beta\gamma$ hENaCs (relative current = 1.19 ± 0.01, $n = 7$, $p < 0.001$; Fig. 6*A*) as reported by Collier and Snyder (8). At pH 6.0, we observed a minimal inhibitory effect of 10 μM Cu^{2+} ($I_{Cu}/I = 0.86 \pm 0.01$, $n = 7$, $p < 0.001$), in contrast to the large inhibitory effect at pH 7.4 ($p < 0.001$; Fig. 6*B*). These results demonstrate that Cu^{2+} inhibition of hENaC is pH-dependent and are consistent with His side chains mediating the interaction of Cu^{2+} with hENaC.

There are 10, 13, and 14 His residues in the ECDs of α, β, and γ hENaC, respectively. We individually mutated each His residue to identify other sites for Cu^{2+} interaction with the chan-

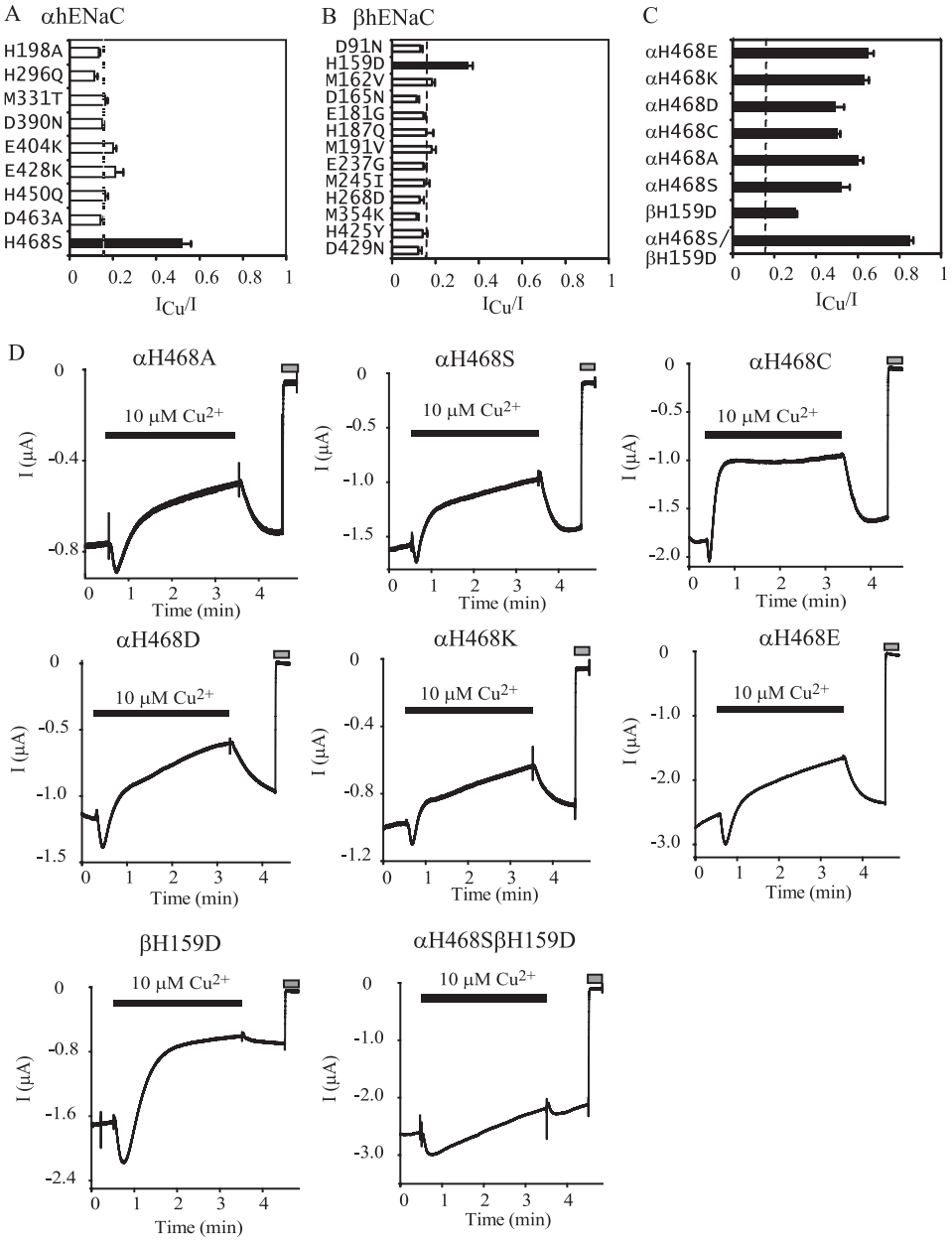

FIGURE 5. **Identification of αHis^{468} and βHis^{159} as potential sites mediating Cu^{2+} interaction with hENaCs.** Point or double mutations were introduced in one hENaC subunit, which was co-expressed with other WT hENaC subunits. Mutational sites were selected to substitute nonconserved residues capable of binding Cu^{2+} in α or β hENaC subunits with their corresponding residues in α or β mENaC-based on sequence alignments. *A*, I_{Cu}/I at 10 μM Cu^{2+} from oocytes expressing mutant α and WT β and γ hENaCs ($n = 5$). The I_{Cu}/I values in this and all other subsequent figures were obtained in the same way as in Fig. 4*F*. *B*, I_{Cu}/I from oocytes expressing mutant β and WT α and γ hENaCs ($n = 5$ except $n = 4$ for D91N and D429N). *C*, I_{Cu}/I from oocytes expressing αHis^{468} mutants and αH468S/βH159D ($n = 5$–7). The *black bars* in *A*–*C* indicate that the values were significantly different from that of WT $\alpha\beta\gamma$ hENaCs obtained in the same batches of oocytes ($p < 0.01$). The *dashed line* shows the average I_{Cu}/I values from all oocytes expressing WT $\alpha\beta\gamma$ hENaCs used in this experiment (0.15 ± 0.00, $n = 164$) for reference only but not for statistical significance analyses. *D*, representative recordings showing the effect of 10 μM Cu^{2+} on mutant hENaCs. The *gray bars* indicate the times when 10 μM amiloride was present. Bath solution was buffered with 10 mM HEPES.

nel. In addition to the αHis^{468} mutants (Fig. 5), substitution of αHis^{255} with Ala, Cys, Asp, or Arg significantly reduced channel inhibition by 10 μM Cu^{2+} (Fig. 7*A*). For the β subunit, two mutations (βH159A and βH160A) significantly reduced Cu^{2+} inhibition (Fig. 7*B*). The change in Cu^{2+} inhibition by βH159A was similar to that of βH159D (Fig. 5*B*). Two γ His mutants (γH88A and γH277A) showed a significantly reduced inhibitory effect of 10 μM Cu^{2+} (Fig. 7*C*). We also noted that substitutions at two γECD sites (γHis^{233} and γHis^{332}) increased the inhibitory effect of 10 μM Cu^{2+} ($p < 0.01$).

We examined whether mutations of His residues in multiple subunits would enhance the loss of the inhibitory effect of 10 μM Cu^{2+}, as we observed with the αH468SβH159D mutant (Fig. 5). Double mutations such as αH468A/βH160A ($I_{Cu}/I = 1.01 \pm 0.02$, $n = 5$, $p < 0.0001$ *versus* WT) and αH468A/γH277A ($I_{Cu}/I = 0.97 \pm 0.03$, $n = 4$, $p < 0.0001$ *versus* WT) eliminated inhibitory effect of 10 μM Cu^{2+}. In contrast, βH159AγH277A greatly reduced but did not eliminate 10 μM Cu^{2+} inhibition ($I_{Cu}/I = 0.48 \pm 0.03$, $n = 5$, $p < 0.0001$ *versus* WT; Fig. 8). These data suggest that αHis^{468} is

TABLE 2

Time constants for current changes during (application, 3 min) and after (washout, 1 min) 10 μM Cu^{2+} applications in oocytes expressing WT or mutant hENaC

Time constants were obtained from best fit of the current changes using built-in exponential function in Clampfit 10. The values for WT hENaC were pooled from all oocytes of different batches for reference only. Statistical tests were performed by comparing the values from WT and mutants obtained in the same batches of similar numbers of oocytes. ND, not determined.

hENaC	Application	Washout	Oocytes
	s	*s*	
WT	27.1 ± 0.8	50.0 ± 7.3	67
αH255A	21.3 ± 1.7	36.0 ± 6.0	5
αH255C	33.9 ± 3.4	35.9 ± 6.0	5
αH255D	29.4 ± 1.5	21.5 ± 4.7	6
αH255R	27.0 ± 2.1	44.3 ± 7.7	5
αH468A	32.4 ± 3.3	14.7 ± 1.4[a]	5
αH468C	10.2 ± 1.5[a]	15.6 ± 1.3[a]	5
αH468D	46.4 ± 4.6[a]	31.0 ± 3.4	5
αH468E	64.6 ± 6.7[a]	17.3 ± 3.2	4
αH468K	49.6 ± 3.2[a]	32.4 ± 3.7	7
αH468S	23.7 ± 3.8	27.6 ± 2.5[a]	5
βH159A	29.7 ± 2.5	18.3 ± 2.6	6
βH159D	34.1 ± 2.0	17.7 ± 3.2	5
βH160A	28.9 ± 1.3	64.1 ± 5.9	5
βE254A	29.5 ± 2.3	24.8 ± 3.9	5
βE254C	38.1 ± 1.9	22.7 ± 2.5	5
βE254D	33.7 ± 3.8	22.0 ± 3.3	5
βE254H	33.5 ± 2.0	22.0 ± 1.7	5
βE254Q	28.5 ± 2.1	20.6 ± 2.6	5
βE254R	32.2 ± 2.9	16.9 ± 2.6	5
γH88A	38.5 ± 3.1	44.0 ± 4.6	5
γH233A	18.3 ± 2.1	ND	5
γH233C	21.6 ± 2.2	ND	5
γH233D	13.0 ± 1.8[a]	ND	5
γH233R	22.5 ± 2.4[a]	ND	5
γH277A	35.9 ± 1.1	18.3 ± 1.7[a]	5
γH332A	17.1 ± 0.4[a]	ND	5

[a] The values were significantly different from that of WT in the same batch of oocytes ($p < 0.01$).

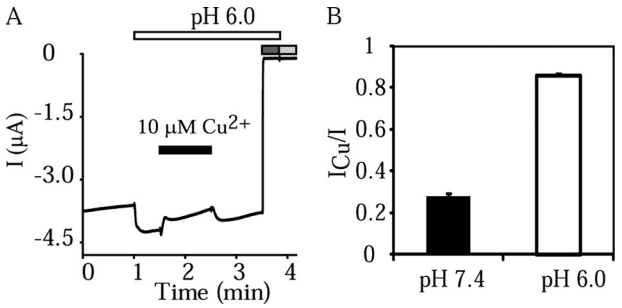

FIGURE 6. **Lowering pH of bath solution diminishes the inhibitory effect of Cu^{2+}.** Oocytes expressing WT αβγ hENaCs were clamped at −100 mV. *A*, a typical recording showing the effects of lowering bath solution pH from 7.4 (buffered with 5 mM MES and 5 mM MOPS) to 6.0 (buffered with 10 mM MES) on the base-line current and Cu^{2+} inhibition at 10 μM. The *dark* and *light gray bars* indicate the time periods in the presence of 10 μM amiloride in pH 6.0 and 7.4, respectively. There was no difference between the currents with amiloride at pH of 6.0 and 7.4. *B*, I_{Cu}/I at pH 7.4 and 6.0 ($n = 7$, $p < 0.001$). A control experiment at pH 7.4 was performed in the same way as in Fig. 2*A*. In experiments with both pH 6.0 and 7.4, 10 μM Cu^{2+} was applied for only 1 min to minimize potential complication from intracellular acidification, which inhibits ENaCs (47). The I_{Cu}/I obtained with 1 min of application of 10 μM Cu^{2+} at pH 7.4 was slightly greater than that with 3 min of application.

a key site for conferring the inhibitory effect of external Cu^{2+}.

A Cu^{2+} Binding Site Is Located at a Subunit Interface—In certain ligand-gated channels, transition metal-binding sites are located at subunit interfaces (33, 34). We reasoned that external Cu^{2+} might bind at a contact site between two subunits. Residue αHis^{468} aligned with Lys^{355} of cASIC1. The cASIC1 structure shows that the side chain of Lys^{355}, located at

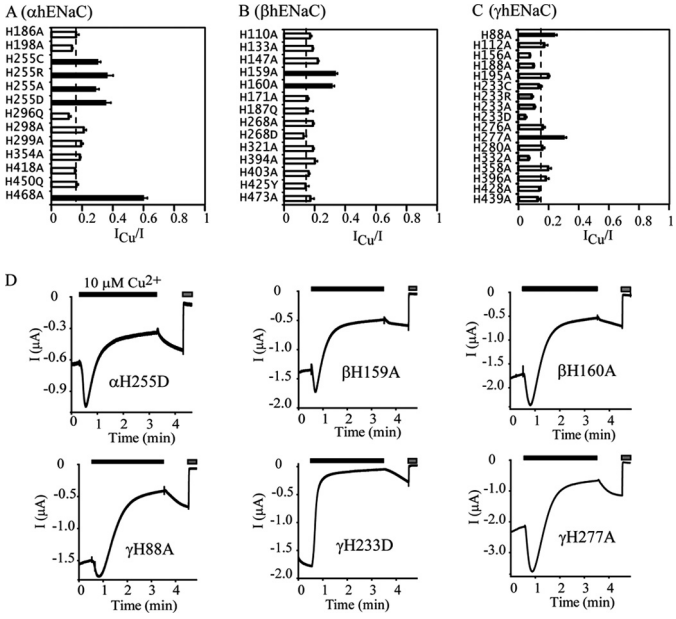

FIGURE 7. **Mutations of multiple His residues within the ECDs reduce the inhibitory effect of Cu^{2+} on hENaCs.** The I_{Cu}/I values reflecting the magnitudes of the inhibitory effect of 10 μM Cu^{2+} were obtained from oocytes expressing mutant α together with WT β and γ hENaCs (*A*), mutant β with WT α and γ hENaCs (*B*), or mutant γ with WT α and β hENaCs (*C*). *Black bars* in *A–C* indicate that the values were significantly greater than that of WT αβγ hENaCs obtained in the same batches of oocytes ($p < 0.01$, $n = 5$ for both mutants and WT). The values in γH233R, γH233A, γH233D, and γH332A (*gray bars*) were significantly less than that of WT ($p < 0.01$). The *dashed line* shows the average I_{Cu}/I value from all oocytes expressing WT αβγ hENaCs used in this experiment (0.15 ± 0.00, $n = 164$) for reference only but not for statistical significance analyses. I_{Cu}/I for αH468A was from Fig. 5*C* and is shown for comparison. *D*, representative recordings of currents with 3-min applications of 10 μM Cu^{2+}. The *gray bars* in *D* indicate the presence of 10 μM amiloride. Bath solution was buffered with 10 mM HEPES.

the carboxyl end of an α helix (α5) in the thumb domain interacts with side chain of Glu^{178} within the β3-β4 loop of the palm domain of an adjacent subunit (Fig. 9*A*) (13). The distance between NZ of Lys^{355} and OE2 of Glu^{178} is 3.2 Å, well within the range of distance for ion pairs in proteins (35). Lys^{355} of cASIC1 aligns with hENaC αHis^{468}, βArg^{437}, and γGlu^{446}, whereas Glu^{178} of cASIC1 aligns with hENaC αVal^{287}, βGlu^{254}, and γVal^{265} (Fig. 9*C*). Of these six hENaC residues, only αHis^{468} and βGlu^{254} could form an ion pair. If a His residue resides at the position of Lys^{355} in subunit A of cASIC1, the distances between an imidazole nitrogen of Lys^{355} and a carboxyl oxygen of Glu^{178} in subunit C of cASIC1 would be 3.4–5.5 Å, close to the sum of average distances for Cu^{2+}-N-His (2.0∼2.1 Å) and Cu^{2+}-O-Glu (2.2 Å) in proteins (36). We therefore hypothesized that αHis^{468} and βGlu^{254} coordinate the same Cu^{2+} at the α and β subunit interface. To test the hypothesis, we mutated βGlu^{254} to Ala, Arg, Gln, His, Asp, and Cys. All of the substitutions except βE254D led to a modest but significant reduction of inhibition by 10 μM Cu^{2+} (Fig. 9*D*). The double mutant αH468A/βE254A nearly eliminated the inhibitory effect of 10 μM Cu^{2+} ($I_{Cu}/I = 0.83 \pm 0.01$, $n = 5$, $p < 0.0001$ *versus* WT, αH468A or βE254A; Fig. 9*E*). Our observations are consistent with the above hypothesis that αHis^{468} and βGlu^{254} contribute to coordination of the same Cu^{2+} ion. The close proximity of αHis^{468} and βGlu^{254} requires an obligate counterclockwise subunit arrangement of α-β-γ when viewed from above (Fig.

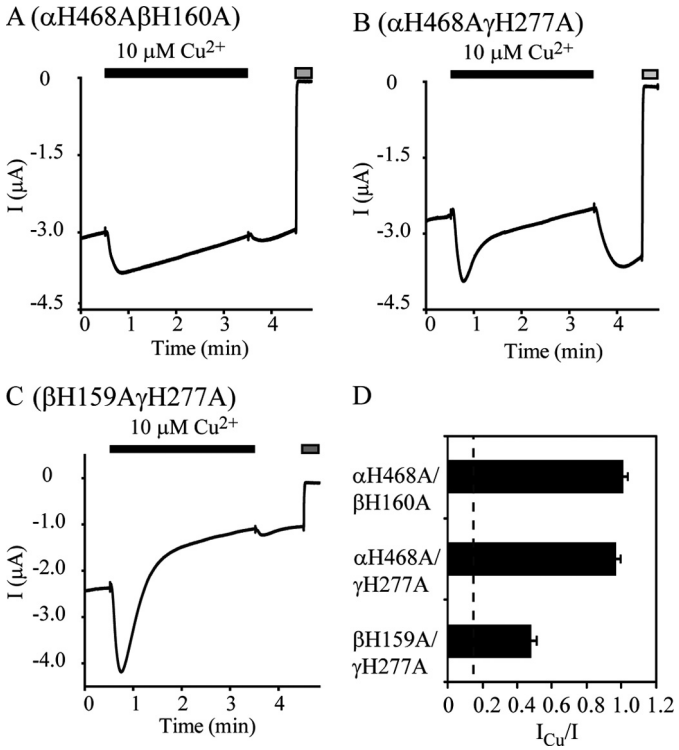

FIGURE 8. **Double mutations of αHis^{468} and βHis^{160} or γHis^{277} eliminate the inhibitory effect of 10 μM Cu^{2+} on hENaCs.** Oocytes expressing two mutant hENaC subunits and one WT hENaC subunit were clamped to −100 mV. The effects of 10 μM Cu^{2+} were examined together with WT αβγ hENaCs in the same way as in previous figures. *A–C*, representative recordings showing the responses of the double mutants to 10 μM Cu^{2+}. *Gray bars* show the presence of 10 μM amiloride. *D*, I_{Cu}/I obtained from four or five oocytes expressing the double mutants. *Black bars* show that the values were significantly different from that of WT obtained in the same batches of oocytes ($p < 0.001$). The *dashed line* shows the average I_{Cu}/I from all WT expressing oocytes used in this particular experiment (0.16 ± 0.01, $n = 19$) for the purpose of reference. Bath solution was buffered with 10 mM HEPES.

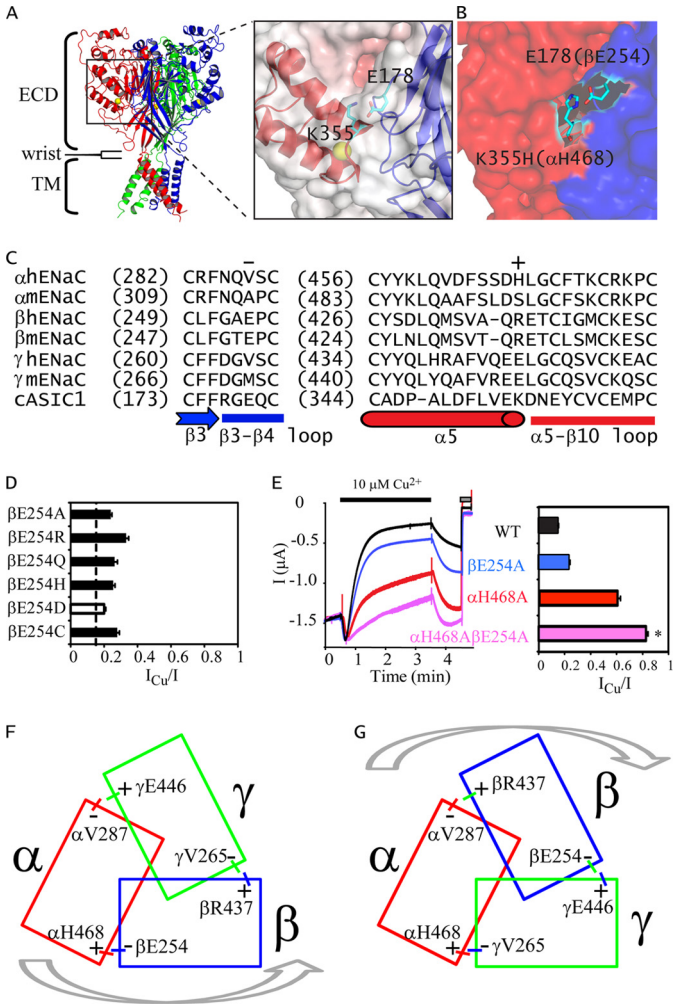

FIGURE 9. **Identification of αHis^{468} and βGlu^{254} pair at subunit interface.** *A*, a structural model of chicken ASIC1. The trimeric cASIC1 structure (45) was rendered as three colored ribbons (subunit A, B, and C in *red*, *green*, and *blue*, respectively) with PyMol (version 1.3) using coordinates from Protein Data Bank (identification code 3HGC). The ECDs on the top part of the structure are linked to the transmembrane (*TM*) domain via six short coiled segments termed the wrist (13). The *boxed area* is enlarged on the *right* to show the contact between the thumb domain Lys^{355} of subunit A and the palm domain Glu^{178} of subunit C in the cASIC1 structure. For clarity the area is shown with semitransparent surface and ribbon rendering. The side chains of Lys^{355} and Glu^{178} are shown as sticks with carbon, oxygen, and nitrogen atoms colored in *cyan*, *red*, and *blue*, respectively. *B*, nontransparent surface rendering of the same region as in *A* with subunit A in *red* and subunit C in *blue* to highlight the subunit interface. Lys^{355} was mutated to a His. Homologous hENaC residues to K355H and Glu^{178} are shown in *parentheses*. The surface near the two residues are omitted. *C*, sequence alignments of human, mouse ENaCs, and cASIC1 in regions surrounding βGlu^{254} (−) and αHis^{468} (+). Secondary structures are shown according to the cASIC1 structure (13). *D*, I_{Cu}/I from oocytes expressing β mutant and WT α and γ hENaCs. *Black bars* indicate that the values were significantly different from that of WT in the same batches of oocytes ($p < 0.01$, $n = 5$). The *dashed line* shows the average value from pooled WT-expressing oocytes in this experiment (0.16 ± 0.01, $n = 10$). Bath solution was buffered with 10 mM HEPES. *E*, superimposed traces showing the responses of WT (*black*), βE254A (*blue*), αH468A (*red*), and αH468A/βE254A (*purple*) and I_{Cu}/I values in corresponding colors. All of the mutant values were significantly greater than that of WT ($p < 0.001$), and the *asterisk* shows that the value of the double mutant was significantly greater than that of the either single mutant ($p < 0.001$, $n = 5$). *F*, an illustration showing a counterclockwise arrangement of three ENaC subunits in a *top view*. Three *rectangles* represent the approximate spaces occupied by α (*red*), β (*blue*), and γ (*green*) subunits. Overlapped regions highlight intersubunit contacts including three-way interaction at the center and two-way interactions at more distal regions. Subunit-subunit interactions happen primarily along the two inner laterals. We designated the long inner sides as + and the short inner side as − by convention used in other ligand-gated channels. *G*, an alternative (clockwise) arrangement of α, β, and γ ENaC subunits.

9*F*). A clockwise arrangement of α, β, and γ subunits would place γGlu^{446} and βGlu^{254} in close proximity (Fig. 9*G*). Charge reversal mutation γE446R did not alter the inhibitory effect of 10 μM Cu^{2+} ($I_{Cu}/I = 0.08 \pm 0.01$, $n = 4$, $p > 0.7$ *versus* WT). The result was not consistent with an involvement of γGlu^{446} in Cu^{2+} binding and a pairing between γGlu^{446} and βGlu^{254} that would otherwise require a clockwise organization of α, β, and γ subunits.

Cu^{2+} Inhibition and Na^+ Self-inhibition—We studied the effect of Cu^{2+} on hENaC in a bath solution containing 110 mM Na^+, which is typically used by investigators so as to produce easily measurable currents. At this concentration, extracellular Na^+ reduces the P_o of ENaC via a process of Na^+ self-inhibition (25, 26, 37, 38). The degree of Na^+ self-inhibition dramatically affects the effects of other extracellular regulators on ENaCs such as Zn^{2+}, H^+, and Cl^- (7–9). We suspected that some of the six His mutations might alter the Na^+ self-inhibition response, and as a secondary effect Cu^{2+} inhibition appeared to be reduced. We therefore examined the Na^+ self-inhibition responses of these mutant ENaCs.

As shown in Fig. 10, αH255A greatly enhanced Na^+ self-inhibition, whereas βE254Q and γH277A moderately increased the magnitude of Na^+ self-inhibition. In contrast, αH468A, βH159A, βH160A, and γH88A did not significantly

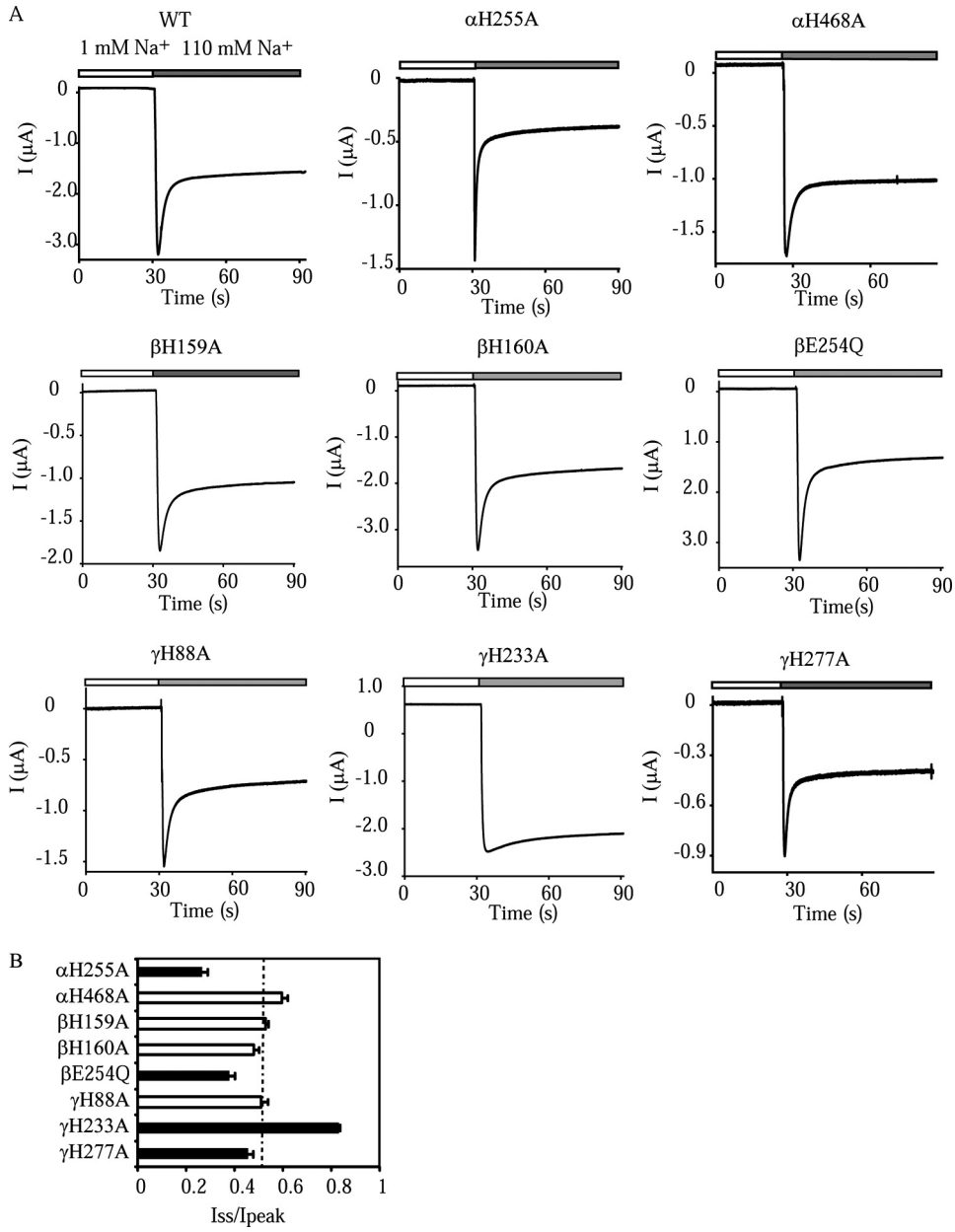

FIGURE 10. **Na^+ self-inhibition responses of mutant hENaCs.** *A*, representative traces showing Na^+ self-inhibition responses of WT and αH255A, αH468A, βH159A, βH160A, βE254Q, γH88A, γH233A, and γH277A mutants. The oocytes were clamped at −100 mV, and the whole cell currents were continuously recorded, whereas bath [Na^+] was rapidly increased from 1 mM (*open bar*) to 110 mM (*gray bar*). Both bath solutions were buffered with 10 mM HEPES. The traces are representative of at least five independent observations. The current decay following an increase in [Na^+] represents Na^+ self-inhibition. *B*, I_{ss}/I_{peak} of mutant hENaCs. I_{peak} was the peak current, and I_{ss} was the current 40 s after the peak current. The ratio is inversely proportional to the magnitude of Na^+ self-inhibition. The *black bars* indicate that values were significantly different from that of WT obtained in the same batches of oocytes ($p < 0.01$, $n = 5$). The *dashed line* indicates the average value of WT hENaCs pooled from all oocytes in this experiment (0.50 ± 0.01, $n = 84$) for reference only.

change the Na^+ self-inhibition response. Na^+ self-inhibition was largely eliminated in the γH233A mutant, as previously reported (8). These observations suggest that αHis^{468}, βHis^{159}, βHis^{160}, and γHis^{88} have specific roles in Cu^{2+} inhibition of hENaC.

Mutations that altered the Na^+ self-inhibition response also changed the magnitude of the transient activation of current that appeared before the inhibitory effect of Cu^{2+} (Figs. 1*A* and 7*D*). The transient activation was absent in mutants with Na^+ self-inhibition eliminated (for example, γH233D; Fig. 7*D*). It suggests that the transient activation by Cu^{2+} was caused by a relief of Na^+ self-inhibition, in a manner similar to that of ENaC activation by external Zn^{2+} and H^+ (7, 8). Accordingly, αH255D and γH277A that enhanced the Na^+ self-inhibition response increased the magnitude of the transient Cu^{2+} activation by 5.3- and 3.1-fold, respectively, compared with WT ($p < 0.001$). These observations suggest that the reduced Cu^{2+} inhibition in αHis^{255} and γHis^{277} mutants (*i.e.* greater I_{Cu}/I; Fig. 7) was related to the augmented stimulatory effect of Cu^{2+}, which resulted from enhanced Na^+ self-inhibition. Other mutations including αHis^{468} mutations (Fig. 5*D*), βH159A (Fig. 7*D*), βH160A (Fig. 7*D*), βGlu^{254} mutations (Fig. 9*E*), and γH88A (Fig. 7*D*) did not significantly change the transient Cu^{2+} stimulation, consistent with their specific role in the inhibitory effect of Cu^{2+}.

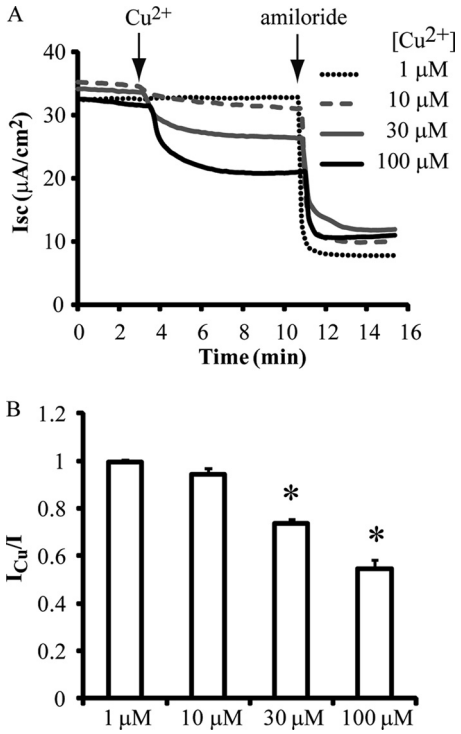

FIGURE 11. **Cu^{2+} inhibits native human ENaCs in human airway epithelial cells.** *A*, superimposed short circuit recordings showing the responses of the currents to 1, 10, 30, and 100 μM Cu^{2+} applied in apical chamber. *B*, I_{Cu}/I, ratio of amiloride-sensitive current in the presence of Cu^{2+} and amiloride-sensitive current prior to Cu^{2+} application. The *asterisks* indicate that the values in the presence of 30 and 100 μM Cu^{2+} were significantly less than that of base-line currents ($p < 0.001$, $n = 6$).

Cu^{2+} Inhibits Short Circuit Current in Human Airway Epithelial Monolayers—We studied whether external Cu^{2+} had an inhibitory effect on natively expressed human ENaCs similar to that on cloned ENaCs expressed in oocytes by examining the effect of apically applied Cu^{2+} on the short circuit currents in human airway epithelial monolayers. The portion of I_{sc} that was blocked by 10 μM amiloride was considered ENaC-mediated current. As shown in Fig. 11, Cu^{2+} at doses above 10 μM reduced the I_{sc} in a dose-dependent manner.

DISCUSSION

In this study, we found that external Cu^{2+} inhibited human $\alpha\beta\gamma$ ENaC in both *Xenopus* oocytes and human airway epithelia. External Cu^{2+} at 10 μM does not inhibit mouse (Fig. 4) or rat ENaC.[3] Native *Xenopus* ENaCs in A6 cells are activated by extracellular Cu^{2+} (14). Therefore, in the context of previous reports and our current observations, external Cu^{2+} appears to be a specific inhibitor of human ENaC among cloned ENaCs. The inhibitory effect of Cu^{2+} on the hENaC current in the human airway epithelia appeared to be smaller and weaker than that in oocytes (Fig. 11). We do not know the exact cause for the different responses to Cu^{2+}. They could be related to certain experimental conditions utilized in the two systems, such as temperatures (*i.e.* 20–24 °C in oocytes and 37 °C in epithelia) and oxygen tensions, both of which regulate ENaC activity (25, 39, 40). The differences in the response to Cu^{2+} could also reflect the inherent differences between native and heterologously expressed channels. It has been reported that ENaCs in oocytes and epithelial monolayers display different sensitivities to the peptide inhibitors derived from the inhibitory domains of α and γ mouse ENaCs (41, 42).

The estimated IC_{50} of 0.31 μM for Cu^{2+} inhibition suggests that external Cu^{2+} is a potent hENaC inhibitor. A high affinity ENaC inhibitor may be useful in treating diseases associated with elevated ENaC-mediated Na^+ absorption such as Liddle syndrome and cystic fibrosis (43, 44).

Recent studies have established a critical role for ENaCs in the regulation of airway surface liquid volume and excessive activity of ENaCs in airways contributes to the pathogenesis of cystic fibrosis (44). Impaired Na^+ transport in alveoli leads to pulmonary edema (40). Airborne particles contain a considerate amount of transition metals including copper. Upon contact with biological fluids, free metal ions can be released from the particles and cause local and even remote toxic effects (17, 18). We speculate that the inhibitory effect of Cu^{2+} on human ENaCs in lung epithelia may contribute to the toxicological symptoms caused by inhaled particulate matters. Cu^{2+}, released from particulate matters, may worsen particle-induced pulmonary edema by inhibition of Na^+ absorption in airways and alveoli.

The main goal of this study was to probe the structural basis for hENaC inhibition by external Cu^{2+}. Experiments with mixed human and mouse ENaC subunits demonstrate that α and β hENaC subunits are necessary for the specific response of hENaCs to Cu^{2+} (Fig. 4). Initial mutational screening of the hENaC-specific residues within α and β ECDs identified αHis^{468} and βHis^{159} as residues involved in Cu^{2+} inhibition (Fig. 5). The double mutant (αH468S-βH159D) converted the response to Cu^{2+} of the human channel to that of the mouse channel (Figs. 4 and 5), suggesting that these two hENaC-specific residues are primarily responsible for the distinct response to 10 μM Cu^{2+} of human *versus* mouse ENaC. Subsequently, systematic screening of His residues within ECDs of α, β, and γ subunits identified additional four sites (αHis^{255}, βHis^{160}, γHis^{88}, and γHis^{277}) where mutations significantly reduced the inhibitory effect of 10 μM Cu^{2+} (Fig. 7). However, further analyses showed that αHis^{255} and γHis^{277} mutations significantly increased the magnitudes of Na^+ self-inhibition and Cu^{2+}-induced transient activation preceding the inhibitory effect (Figs. 7*D* and 10), suggesting indirect roles for both His residues in the Cu^{2+} inhibition. Another residue, γHis^{88}, does not appear to have an essential role in Cu^{2+} inhibition, given the small effect of its mutation on Cu^{2+} inhibition (Fig. 7). On the contrary, αHis^{468}, βHis^{159}, and βHis^{160} mutations specifically reduced Cu^{2+} inhibition, without affecting the Na^+ self-inhibition response and the transient activation by Cu^{2+}. We conclude that these three His residues are involved in Cu^{2+} inhibition.

Our data suggest that αHis^{468} has a key role in mediating Cu^{2+} inhibition. Taking advantage of the structural information for cASIC1 (13, 45), we predicted that αHis^{468} and βGlu^{254} could contribute to a Cu^{2+}-binding site at the α/β subunit interface. Mutational analyses confirmed the prediction (Fig. 9). The identification of αHis$^{468}/\beta$Glu^{254} pair suggests a counterclockwise configuration of α, β, and γ subunits when viewed

[3] J. Chen and S. Sheng, unpublished observations.

from above the channel (Fig. 9*F*). This subunit arrangement is in agreement with a recent report by Collier and Snyder (46). However, we cannot rule out the presence of both the counterclockwise and clockwise subunit arrangements. Another limitation of the notion is that it is based on the assumption that ENaC, like ASIC1, has a trimeric architecture, which remains to be established experimentally.

ENaC P_o is regulated by a variety of extracellular factors that may share common pathways in their regulation of ENaC gating. Indeed, the effects of external Zn^{2+}, H^+, and Cl^- on ENaC activity rely on the existence of Na^+ self-inhibition (7–9). However, Cu^{2+} inhibition of hENaC does not depend on the existence of Na^+ self-inhibition. In fact, the magnitude of Cu^{2+} inhibition was increased by Na^+ self-inhibition eliminating mutation (γH233A) and reduced by Na^+ self-inhibition enhancing mutation (αH255A). Therefore, Cu^{2+} likely inhibits the hENaC via a pathway distinct from that of Na^+ self-inhibition. In contrast, the transient activation of hENaC by Cu^{2+} appears to result from a relief of Na^+ self-inhibition, because Na^+ self-inhibition eliminating (γH233A) or enhancing (αH255A) mutations diminished or enhanced its magnitude accordingly.

In summary, we found that external Cu^{2+} is a high affinity inhibitor of human ENaC and identified a Cu^{2+}-binding site at subunit interface within the extracellular domains. Structure-assisted mutational analyses suggest that a thumb domain His residue of α subunit and a palm domain Glu residue of the β subunit interact with a Cu^{2+} ion. This pairing (αHis^{468}/βGlu^{254}) requires a counterclockwise arrangement of α, β, and γ ENaC subunits when viewed from above.

Acknowledgments—We thank Dr. Thomas R. Kleyman for critical reading and comments on this manuscript, Dr. Joseph Pilewski at the Airway Epithelial Cell Culture Core at the University of Pittsburgh for providing human bronchial epithelial cultures, and Brandon M. Blobner for oocyte preparation.

REFERENCES

1. Sheng, S., Johnson, J. P., and Kleyman, T. R. (2007) in *Seldin and Giebisch's The Kidney: Physiology & Pathophysiology* (Alpern, R. J., and Hebert, S. C., eds.) 4th Ed., pp. 743–768, Academic Press, New York
2. Bhalla, V., and Hallows, K. R. (2008) *J. Am. Soc. Nephrol.* **19,** 1845–1854
3. Passero, C. J., Hughey, R. P., and Kleyman, T. R. (2010) *Curr. Opin. Nephrol. Hypertens* **19,** 13–19
4. Garty, H., and Palmer, L. G. (1997) *Physiol. Rev.* **77,** 359–396
5. Van Driessche, W., and Zeiske, W. (1985) *Physiol. Rev.* **65,** 833–903
6. Sheng, S., Perry, C. J., and Kleyman, T. R. (2002) *J. Biol. Chem.* **277,** 50098–50111
7. Sheng, S., Perry, C. J., and Kleyman, T. R. (2004) *J. Biol. Chem.* **279,** 31687–31696
8. Collier, D. M., and Snyder, P. M. (2009) *J. Biol. Chem.* **284,** 792–798
9. Collier, D. M., and Snyder, P. M. (2009) *J. Biol. Chem.* **284,** 29320–29325
10. Nie, H. G., Zhang, W., Han, D. Y., Li, Q. N., Li, J., Zhao, R. Z., Su, X. F., Peng, J. B., and Ji, H. L. (2010) *Am. J. Physiol. Renal Physiol.* **298,** F323–F334
11. Kleyman, T. R., Carattino, M. D., and Hughey, R. P. (2009) *J. Biol. Chem.* **284,** 20447–20451
12. Carattino, M. D., Sheng, S., and Kleyman, T. R. (2004) *J. Biol. Chem.* **279,** 4120–4126
13. Jasti, J., Furukawa, H., Gonzales, E. B., and Gouaux, E. (2007) *Nature* **449,** 316–323
14. Yu, L., Eaton, D. C., and Helms, M. N. (2007) *Am. J. Physiol. Renal Physiol.* **293,** F236–F244
15. Ellingsen, D. G., Horn, N., and Aaseth, J. (2007) in *Handbook on the Toxicology of Metals* (Nordberg, G. F., Fowler, B. A., Norgberg, M., and Friberg, L. T., eds.) 3rd Ed., pp. 529–547, Academic Press, Burlington, MA
16. Tisato, F., Marzano, C., Porchia, M., Pellei, M., and Santini, C. (2010) *Med. Res. Rev.* **30,** 708–749
17. Adamson, I. Y., Prieditis, H., and Vincent, R. (1999) *Toxicol. Appl. Pharmacol.* **157,** 43–50
18. Prieditis, H., and Adamson, I. Y. (2002) *Exp. Lung Res.* **28,** 563–576
19. Karlsson, H. L., Cronholm, P., Gustafsson, J., and Möller, L. (2008) *Chem. Res. Toxicol.* **21,** 1726–1732
20. Kiss, T., and Osipenko, O. N. (1994) *Pharmacol. Rev.* **46,** 245–267
21. Restrepo-Angulo, I., De Vizcaya-Ruiz, A., and Camacho, J. (2010) *J. Appl. Toxicol.* **30,** 497–512
22. McDonald, F. J., Price, M. P., Snyder, P. M., and Welsh, M. J. (1995) *Am. J. Physiol.* **268,** C1157–C1163
23. McDonald, F. J., Snyder, P. M., McCray, P. B., Jr., and Welsh, M. J. (1994) *Am. J. Physiol.* **266,** L728–L734
24. Hegetschweiler, K., and Saltman, P. (1986) *Inorg. Chem.* **25,** 107–109
25. Chraïbi, A., and Horisberger, J. D. (2002) *J. Gen. Physiol.* **120,** 133–145
26. Sheng, S., Bruns, J. B., and Kleyman, T. R. (2004) *J. Biol. Chem.* **279,** 9743–9749
27. Sheng, S., Maarouf, A. B., Bruns, J. B., Hughey, R. P., and Kleyman, T. R. (2007) *J. Biol. Chem.* **282,** 20180–20190
28. Myerburg, M. M., Harvey, P. R., Heidrich, E. M., Pilewski, J. M., and Butterworth, M. B. (2010) *Am. J. Respir. Cell Mol. Biol.* **43,** 712–719
29. Kellenberger, S., Gautschi, I., Rossier, B. C., and Schild, L. (1998) *J. Clin. Invest.* **101,** 2741–2750
30. Volk, T., Konstas, A. A., Bassalaý, P., Ehmke, H., and Korbmacher, C. (2004) *Pflugers Arch.* **447,** 884–894
31. Dokmanić, I., Sikić, M., and Tomić, S. (2008) *Acta Crystallogr. D Biol. Crystallogr.* **64,** 257–263
32. Pace, C. N., Grimsley, G. R., and Scholtz, J. M. (2009) *J. Biol. Chem.* **284,** 13285–13289
33. Nevin, S. T., Cromer, B. A., Haddrill, J. L., Morton, C. J., Parker, M. W., and Lynch, J. W. (2003) *J. Biol. Chem.* **278,** 28985–28992
34. Nagaya, N., Tittle, R. K., Saar, N., Dellal, S. S., and Hume, R. I. (2005) *J. Biol. Chem.* **280,** 25982–25993
35. Barlow, D. J., and Thornton, J. M. (1983) *J. Mol. Biol.* **168,** 867–885
36. Rulísek, L., and Vondrásek, J. (1998) *J. Inorg. Biochem.* **71,** 115–127
37. Sheng, S., Carattino, M. D., Bruns, J. B., Hughey, R. P., and Kleyman, T. R. (2006) *Am. J. Physiol. Renal Physiol.* **290,** F1488–F1496
38. Maarouf, A. B., Sheng, N., Chen, J., Winarski, K. L., Okumura, S., Carattino, M. D., Boyd, C. R., Kleyman, T. R., and Sheng, S. (2009) *J. Biol. Chem.* **284,** 7756–7765
39. Askwith, C. C., Benson, C. J., Welsh, M. J., and Snyder, P. M. (2001) *Proc. Natl. Acad. Sci. U.S.A.* **98,** 6459–6463
40. Davis, I. C., and Matalon, S. (2007) *Adv. Exp. Med. Biol.* **618,** 127–140
41. Carattino, M. D., Sheng, S., Bruns, J. B., Pilewski, J. M., Hughey, R. P., and Kleyman, T. R. (2006) *J. Biol. Chem.* **281,** 18901–18907
42. Bruns, J. B., Carattino, M. D., Sheng, S., Maarouf, A. B., Weisz, O. A., Pilewski, J. M., Hughey, R. P., and Kleyman, T. R. (2007) *J. Biol. Chem.* **282,** 6153–6160
43. Rossier, B. C., Pradervand, S., Schild, L., and Hummler, E. (2002) *Annu. Rev. Physiol.* **64,** 877–897
44. Donaldson, S. H., and Boucher, R. C. (2007) *Chest* **132,** 1631–1636
45. Gonzales, E. B., Kawate, T., and Gouaux, E. (2009) *Nature* **460,** 599–604
46. Collier, D. M., and Snyder, P. M. (2011) *J. Biol. Chem.* **286,** 6027–6032
47. Chalfant, M. L., Denton, J. S., Berdiev, B. K., Ismailov, II, Benos, D. J., and Stanton, B. A. (1999) *Am. J. Physiol.* **276,** C477–C486